Rheology Behavior of High-Density Polyethylene/Diluent Blends and Fabrication of Hollow-Fiber Membranes via Thermally Induced Phase Separation

Jianli Wang, Liang Wang, Wenxiang Ruan, Cheng Zhang, Jianbing Ji

State Key Laboratory Breeding Base for Green Chemistry Synthesis Technology, College of Chemical Engineering and Materials Science, Zhejiang University of Technology, Hangzhou, China 310014

Received 18 October 2009; accepted 4 April 2010
DOI 10.1002/app.32584
Published online 11 June 2010 in Wiley InterScience (www.interscience.wiley.com).

ABSTRACT: The phase-separation behavior of high-density polyethylene (HDPE)/diluent blends was monitored with a torque variation method (TVM). The torque variation of the molten blends was recorded with a rheometer. It was verified that TVM is an efficient way to detect the thermal phase behavior of a polymer–diluent system. Subsequently, polyethylene hollow-fiber membranes were fabricated from HDPE/dodecanol/soybean oil blends via thermally induced phase separation. Hollow-fiber membranes with a dense outer surface of spherulites were observed. Furthermore, the effects of the spinning temperature, air-gap distance, cold drawing, and HDPE content on the morphology and gas permeability of the resultant membranes were examined. © 2010 Wiley Periodicals, Inc. J Appl Polym Sci 118: 2186–2194, 2010

Key words: membranes; phase behavior; polyethylene (PE)

INTRODUCTION

Recently, thermally induced phase separation (TIPS) has become an extensively used technique for the fabrication of microporous membranes from semicrystalline polymers. Normally, during the TIPS process, a polymer is dissolved in a diluent at an elevated temperature, and the homogeneous polymer solution is cooled to induce solid–liquid or liquid–liquid phase separation.[1–3] The selection of the diluent is one key factor determining the membrane structure. Previous studies have revealed how diluents, such as mineral oil,[2] liquid paraffin,[4–8] and ditridecyl phthalate,[5] affect the structure and performance of polyolefin membranes. Liquid–liquid phase separation is believed to be more favorable for obtaining larger membrane pores. The crystallization temperature is not influenced as much by the diluent. Jeon and Kim[9] studied the phase behavior of polyethylene/soybean oil/dioctyl phthalate ternary blends. These ternary blends exhibited typical upper critical solution temperature phase behavior, and the phase-separation temperature was always higher than that of a polyethylene/soybean oil blend when the diluent mixture was 50 wt % or more soybean oil. Membranes prepared from polyethylene/isoparaffin/soybean oil ternary blends were also investigated by Yoo and Kim.[10]

Once a polymer/diluent system is fixed, the membrane structure is controlled by kinetic factors such as the cooling rate, coagulation temperature, and evaporation time.[11–14] Matsuyama and coworkers[15,16] produced anisotropic and asymmetric polypropylene membranes by controlling the evaporation of diluents from the surface of the melt and the cooling rate gradient across the membranes. Cold drawing is an effective and convenient method for increasing the permeability. Sun et al.[8] studied some major factors of the melt spinning of high-density polyethylene/liquid paraffin (HDPE–LP) blends, which affects the water permeability of high-density polyethylene (HDPE) hollow-fiber membranes. The water permeability increases as the take-up speed increases and the membrane thickness decreases.

The compatibility of the polymeric matrix and the diluent is mainly determined by a visual microscopy method and differential scanning calorimetry.[12] In this work, we used a convenient procedure, the torque variation method (TVM), to determine the phase-separation behavior of an HDPE/diluent system. To the best of our knowledge, the use of TVM for the determination of phase diagrams of membrane solutions has been seldom reported. The phase diagrams of two HDPE blends with liquid

Correspondence to: J. Wang (wangjl@zjut.edu.cn).
Contract grant sponsor: Natural Science Foundation of Zhejiang Province of China; contract grant number: Y4080530.

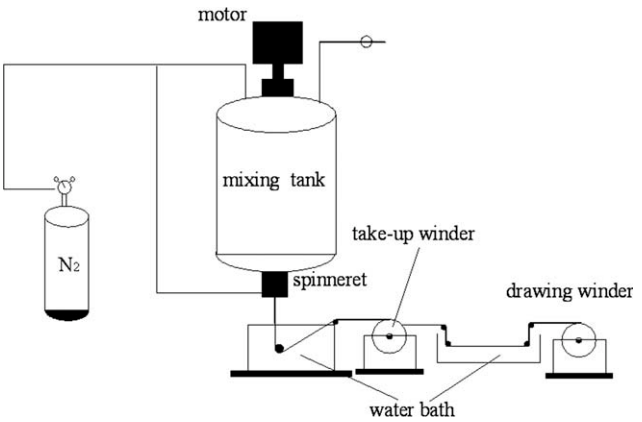

Figure 1 Schematic diagram of the vessel extrusion apparatus for the hollow-fiber membranes.

paraffin and a mixed solvent [1-dodecanol/soybean oil (D/SO) mass ratio = 1 : 1] were compared by TVM. Furthermore, the mixed solvent was used as a diluent to fabricate HDPE hollow-fiber membranes. The effects of the spinning temperature, air-gap distance, cold drawing, and HDPE content on the morphology and gas permeability of the resultant membranes are discussed.

EXPERIMENTAL

Materials

HDPE (5000S; melt flow index = 0.96 g/10 min, density = 0.96 g/cm^3) was supplied by Yangzi Petroleum Co., Ltd. (Nanjing, China) 1-Dodecanol, soybean oil, liquid paraffin, and 2,6-di-*tert*-butyl-4-methylphenol (DTBMP) were commercially available. The ethanol was industrial-grade, and the other reagents were analytically pure. All the reagents were used as received without further purification.

Phase diagram: torque variation

The HDPE, diluent, and antioxidant (DTBMP) were first blended to form a homogeneous solution in a Haake rheometer (Thermo Electron Corp.) (Karlsruhe, Germany) at 190°C with a rotation rate of 40 rpm for 10 min. Then, the chamber was cooled from 190 to 100°C at approximately 3°C/min. The torque of the melt was recorded with the temperature variation. The analysis of the data is described in the Results and Discussion section in detail.

Membrane fabrication and characterization

Polyethylene hollow-fiber membranes were prepared via melt spinning. A vessel extrusion apparatus was designed, as shown in Figure 1. Certain amounts of HDPE and the diluent were placed in the vessel and heated to 185°C under a nitrogen atmosphere to form a homogeneous solution. DTBMP (0.5 wt %) was added as an antioxidant. The homogeneous solution was fed into a spinneret by a gear pump under a nitrogen pressure of 0.2 MPa. The spinneret had outer and inner tubes, and the outer and inner diameters were 1.3 and 0.5 mm, respectively. Another stream of nitrogen was introduced into the spinneret to make a lumen at the center of the fiber. The hollow fiber that extruded from the spinneret was partly cooled in air and was placed in a water bath at 50°C to induce phase separation and solidification by polymer crystallization. The hollow fiber was wound onto a take-up winder at a specified melt draw ratio. The hollow fiber was then wound onto a drawing winder after it passed successively through the take-up winder and a cleaning bath filled with 50°C water. Because the speed of the drawing winder was faster than that of the take-up winder, the hollow fiber was stretched. The drawing ratio was defined as the ratio of the speed of the drawing winder to the speed of the take-up winder. The resulting membrane was successively strain-extracted by ethanol and water for the removal of residual diluents and ethanol and then was dried under the ambient conditions.[6] The preparation conditions for each hollow-fiber membrane are listed in Table I.

The hollow-fiber membranes were fractured in liquid nitrogen and sputtered with gold *in vacuo*. The surfaces and cross sections of the samples were viewed with a Hitachi S-4700(II) (Tokyo, Japan) scanning election microscope.

The membrane porosity (P_r) was determined as follows:

$$P_r = 1 - \frac{W_0}{\rho\pi(D_o^2 - D_i^2)L} \quad (1)$$

where W_0 is the weight of the dried membrane (g); ρ is the density of HDPE (0.96 g/cm^3); D_i and D_o are the inner and outer diameters, respectively (cm); and L is the length of the membrane (cm).

The gas permeability of the membranes was evaluated according to the literature.[17] The nitrogen gas permeability was defined as follows:

TABLE I
Preparation Conditions for the HDPE Hollow-Fiber Membranes

HDPE content (wt %)	30
Mixing temperature (°C)	185
Spinning temperature (°C)	120–145
Air-gap distance (cm)	10–20
Nitrogen supply pressure (cmH_2O)	20
Drawing ratio (%)	110–145
Water-bath temperature (°C)	50

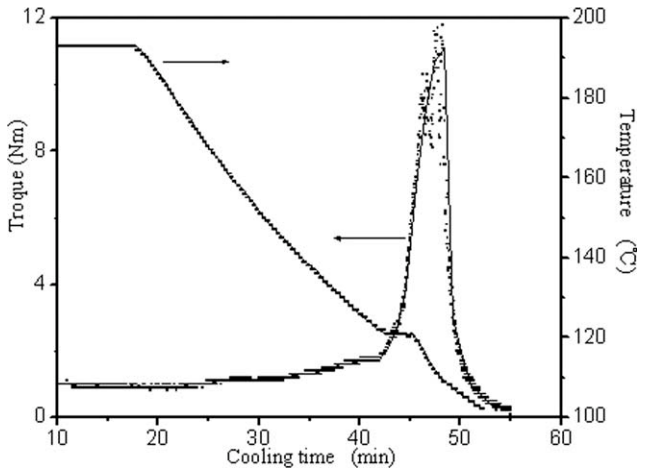

Figure 2 Variation of the torque and temperature for the HDPE–LP (30 wt %) blend under natural cooling conditions.

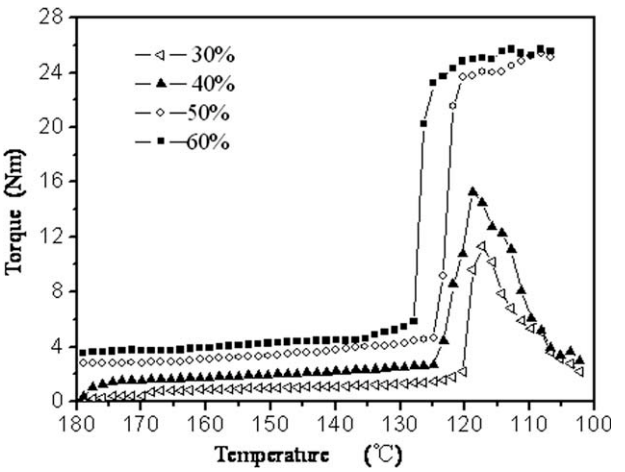

Figure 3 Correlation between the torque and temperature for the HDPE–LP blend.

$$J_g = \frac{V}{\pi L D_i P t} \quad (2)$$

where J_g is the flux of nitrogen through the membrane (cm^3/cm^2 s cmHg), L is the measured fiber length (cm), V is the volume of nitrogen permeating the membrane (cm^3), D_i is the inner diameter of the hollow fiber (cm), P is the pressure difference during the flux test (cmHg), and t is the test time (s).

The length of the membranes was measured with a scale, and the inner and outer diameters were determined with graduated optical microscopy.

RESULTS AND DISCUSSION

Rheology behavior of the polymer solution

HDPE–LP system

In this work, we tried to determine the phase behavior of polyethylene/diluent systems by monitoring the torque and temperature variations of polymer blends with a Haake machine. Typical curves of the torque and temperature for an HDPE–LP (30 wt %) blend with the cooling time are illustrated in Figure 2. The temperature of the blend was almost linearly associated with the cooling time. A slight increase in the torque was accompanied by a progressive decrease in the temperature before 120°C. Successively, a temperature plateau at 120°C, lasting approximately 2 min, indicated that the blend underwent an exothermic stage that possibly contributed to the crystallization of polyethylene. At the same time, the torque increased drastically because of the formation of polymer crystals until this stage was finished.

The correlation between the torque and temperature of HDPE–LP blends with different contents was studied, and the experimental results are presented in Figure 3. Once a blend was cooled to a specific temperature, sharp increases in the torque resulted from the formation of new phases. For 30 and 40 wt % HDPE–LP blends, the torque dropped after a slight increase, which was caused by a complete slip between the polymer blend and screw. In this case, the liquid paraffin worked as a lubricant. In contrast, in 50 and 60 wt % HDPE–LP systems, the more concentrated polymer blend was more difficult to split from the screws, and this resulted in a slow increase in the torque instead of a sharp decrease. This point at which an abrupt change happened was identified as a solid–liquid TIPS point, and the corresponding temperature was considered the crystallization temperature. The locus of the solid–liquid phase-separation point in Figure 3 is plotted in the form of a temperature–composition phase diagram; the curve is called the HDPE–LP phase diagram, as shown in Figure 4. The crystallization temperature increased

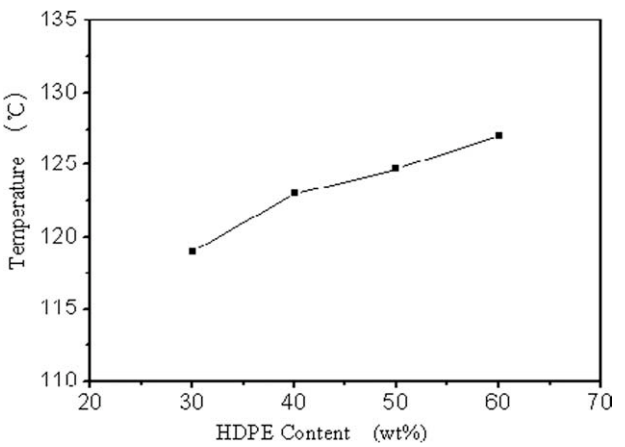

Figure 4 Phase diagram of the HDPE–LP blend determined by TVM.

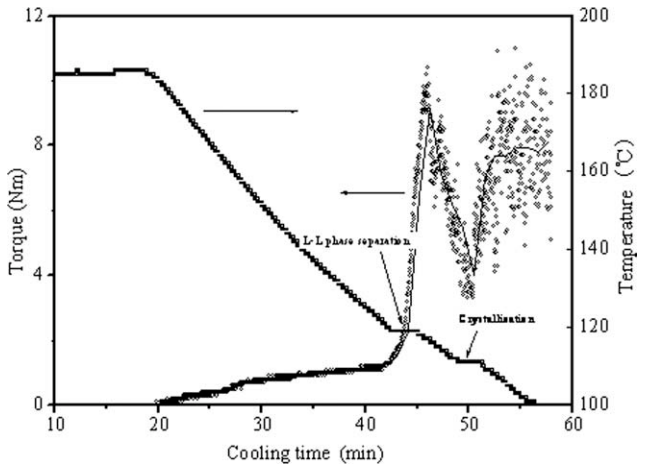

Figure 5 Variation of the torque and temperature of the HDPE–D/SO blend under natural cooling conditions (30 wt %).

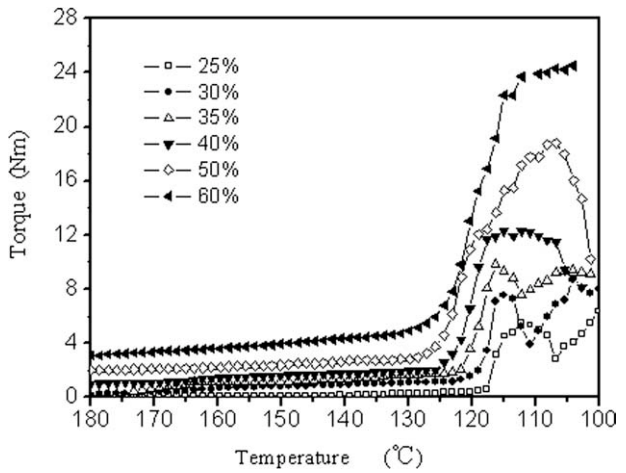

Figure 6 Correlation between the torque and temperature of the HDPE–D/SO blend.

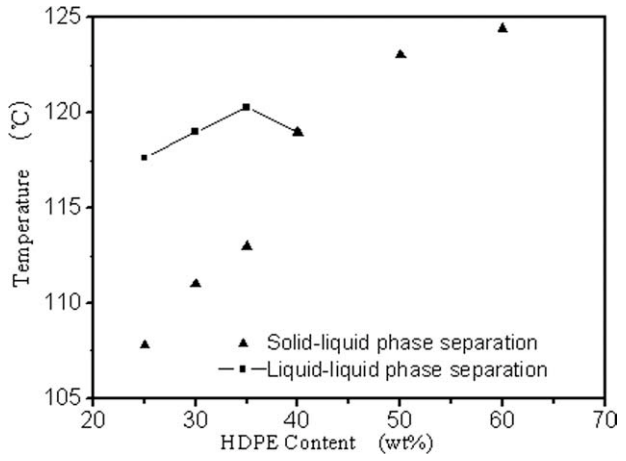

Figure 7 Phase diagram of the HDPE–D/SO blend by TVM.

with the rise in the HDPE concentration. As described by Sun et al.,[4] the HDPE–LP system underwent solid–liquid phase separation.

HDPE–D/SO system

Figure 5 presents the torque variation and temperature versus the cooling time in the HDPE–D/SO system. In this case, unlike the HDPE–LP blend, there were two plateau stages as the temperature of the chamber decreased. The first one, around 120°C, was attributed to liquid–liquid phase separation, and the second stage indicated polymer crystallization. The torque value of the HDPE–D/SO blend

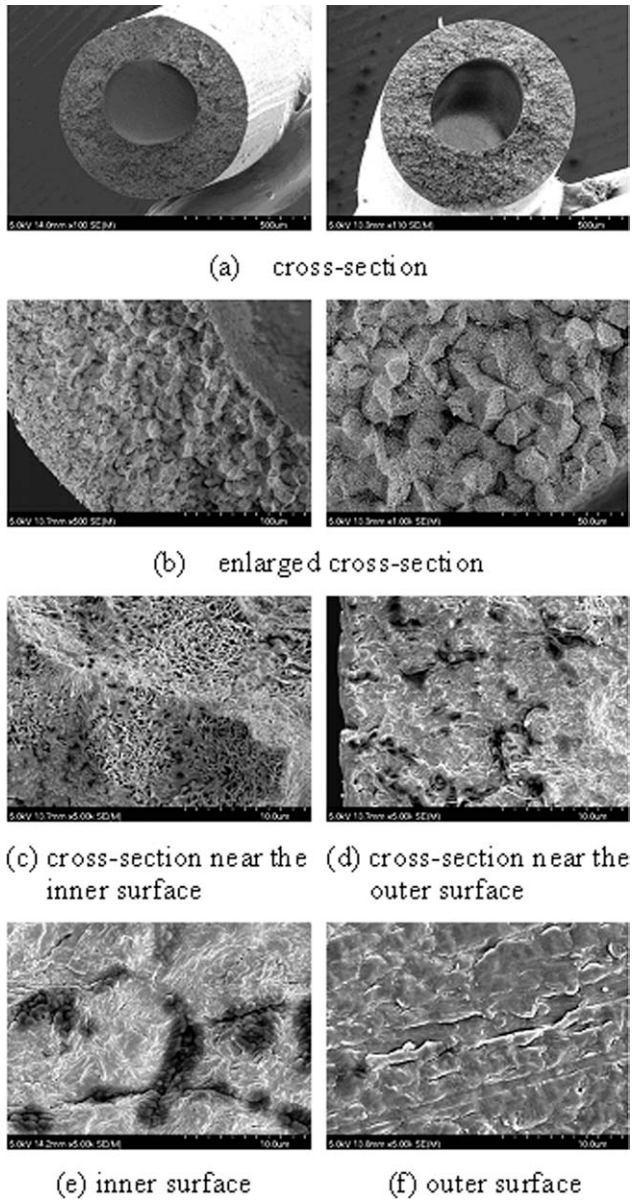

Figure 8 SEM images of the hollow-fiber membranes prepared with the HDPE (30 wt %)–D/SO system (drawing = 100%, air-gap distance = 10 cm, spinneret temperature = 145°C).

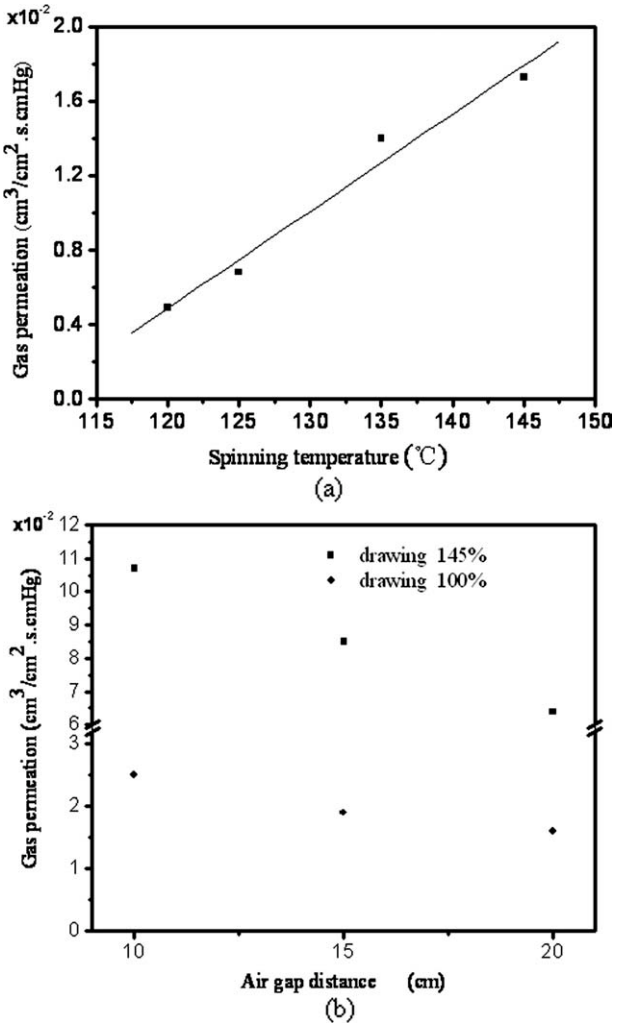

Figure 9 Effect of (a) the spinneret temperature and (b) the air-gap distance on the gas permeation of the hollow-fiber membranes.

underwent two sharp increases, which were attributed to liquid–liquid and solid–liquid phase separation, respectively. These two turning points at which the torque increased abruptly were identified as the liquid–liquid phase-separation temperature and crystallization temperature.

Torque variations versus the temperature for other HDPE–D/SO blends are presented in Figure 6. For 50 and 60 wt % HDPE–D/SO blends, there was only one turning point, which indicated solid–liquid phase separation, whereas two turning points were observed in systems with a concentration below 40 wt %.

The phase diagram, determined by TVM, is shown in Figure 7. Because of the weak interaction between HDPE and D/SO, during cooling, the blending system became unstable and underwent liquid–liquid phase separation; it showed upper critical solution temperature behavior. Torque variations versus the temperature to the left of the monotectic point (initial HDPE concentrations $< 40\%$) showed two rapid increases, which represented liquid–liquid phase separation and solid–liquid phase separation, respectively. There are several disadvantages to using visual microscopy observations in contrast to TVM. First, the phase-separation behavior is not close to the real status of the melt as the cooling rate is fast, and one cannot point out the cloud point easily. Second, it is a static observation, whereas the polymeric melt is processed in a flowing state. However, the phase-separation behavior in a Haake machine is close to the real status of the melt because of its dynamic state.

Membrane structure

Scanning election microscopy (SEM) images of the hollow-fiber membranes obtained from an HDPE–D/SO blend are illustrated in Figure 8. A typical hollow-fiber structure is shown in Figure 8(a). The enlarged cross section shows a membrane consisting

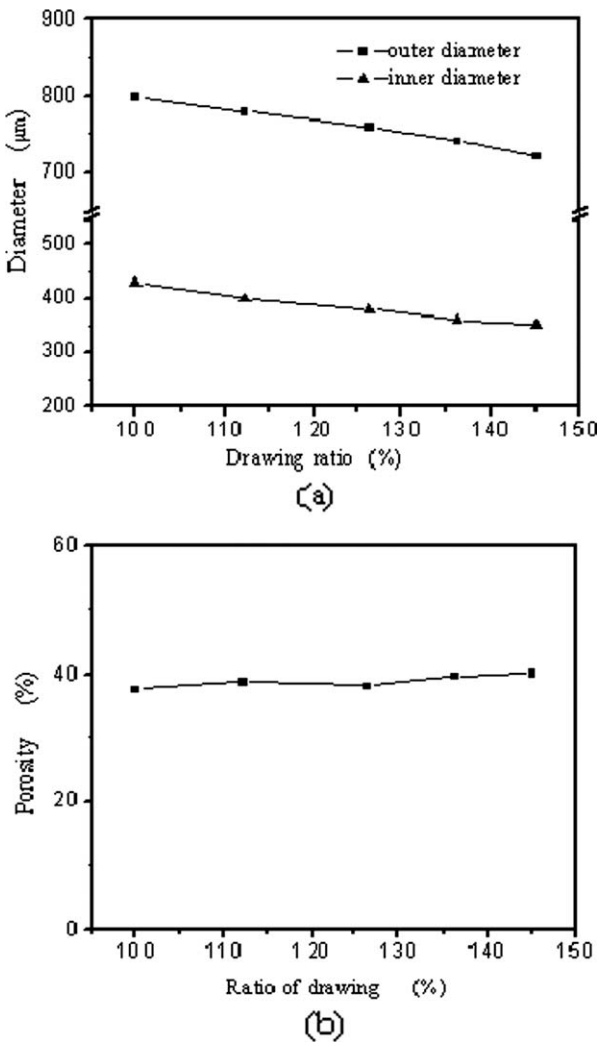

Figure 10 Effect of drawing on (a) the diameter and (b) the porosity of the hollow-fiber membranes.

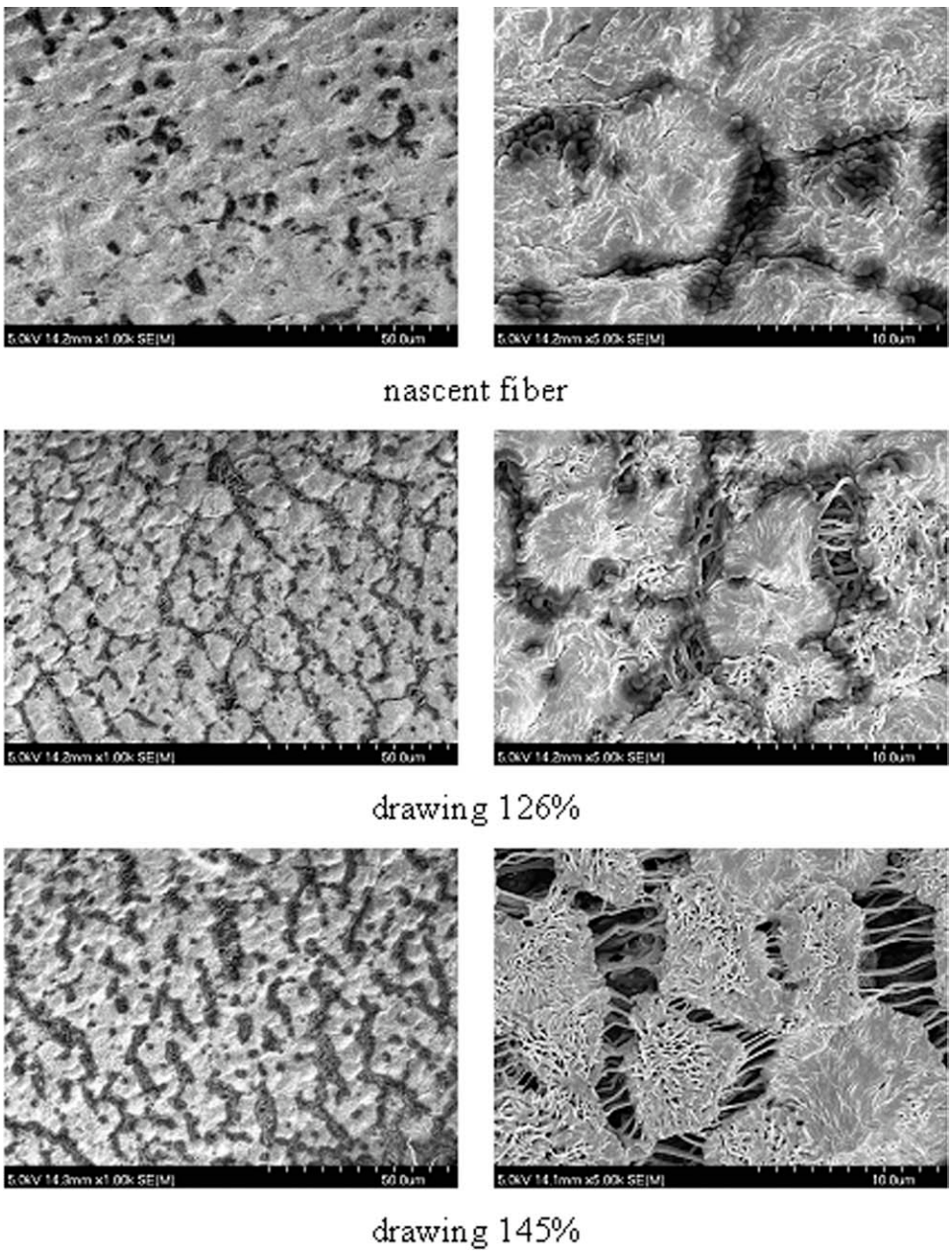

Figure 11 Effect of the drawing ratio on the inner surface of the membrane from the 30 wt % HDPE–D/SO system (air-gap distance = 10 cm, spinneret temperature = 145°C).

of micropores distributed in the spherulites. A comparison of Figure 8(c,d) suggests that an asymmetric membrane with a dense outer surface formed, and the pore size near the inner surface was significantly larger than that near the outer surface. The reason is that the cooling rate of the outer surface, which was exposed to the room environment, was faster than the cooling rate of the inner surface, and this induced the formation of smaller pores near the outer surface. Figure 8(e,f) presents the top and bottom surfaces of the membrane. The outer surface was essentially nonporous. The inner surface was composed of spherical particles, and this indicated that the inner surface was formed by the nucleation and growth of spherulites.

Effects of the spinning temperature and air-gap distance

The impact of the spinning temperature and air-gap distance on the gas permeability of the hollow-fiber membranes from the HDPE–D/SO blend containing 30 wt % HDPE was examined. Above 145°C, the spun fiber melt could not maintain its hollow form and collapsed because of the low viscosity of the melt, whereas below 120°C, the hollow-fiber

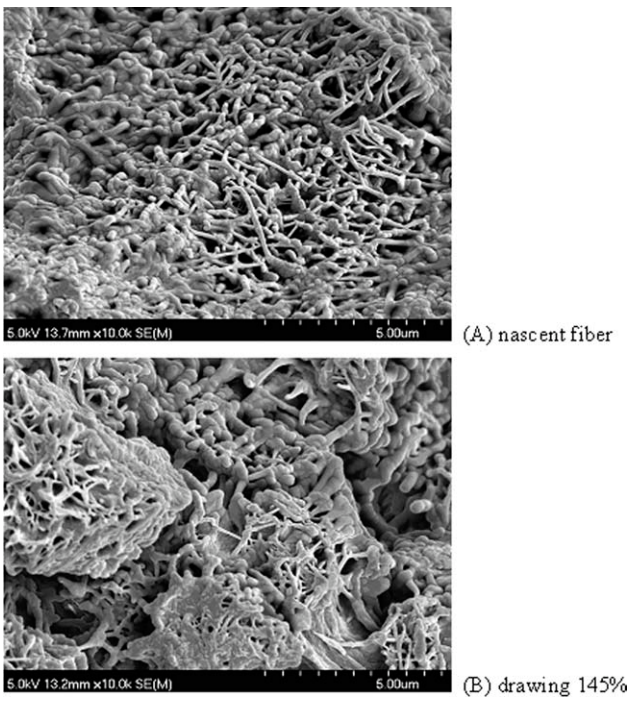

Figure 12 Comparison of the cross-section structures of the membranes from the 30 wt % HDPE–D/SO system fabricated at different drawing ratios (air-gap distance = 10 cm, spinneret temperature = 145°C).

membrane was not uniformly achieved. Therefore, the spinning temperatures discussed here ranged from 120 to 145°C.

Figure 9 implies that the higher gas permeability of the membranes was obtained with a higher spinning temperature and a lower air-gap distance. The lower viscosity, brought about by the higher spinning temperature, was beneficial to the mass transfer between the polymer-rich phase and the polymer-poor phase, and this benefited the liquid–liquid phase separation.

The decrease in the gas permeability with an increase in the air-gap distance was attributed to the increase in the polymer concentration in the surfaces caused by the evaporation of diluents; this agreed with the report by Berghmans et al.[11]

Effect of cold drawing

The effects of the drawing ratio on the inner and outer diameters and porosity of the hollow-fiber membranes are shown in Figure 10. An increase in the drawing ratio led to decreases in the inner and outer diameters because the hollow fibers became more stretched. However, the inner and outer diameter did not change very much because of the highly crystalline character of HDPE. The porosity was little influenced by the drawing ratio under these experimental conditions and rose from 37.6% to 40.2%. When the hollow-fiber membranes were stretched, the microstructure in the axial direction was extended, and this was accompanied by shrinkage in the radial direction. Thus, the porosity and the pore volume were hardly influenced by the drafting force even though the shape of the micropores was changed.

SEM was used to investigate the change in the micropore structures (see Fig. 11). The skin of the nascent fiber was smooth. After the drawing, lots of voids appeared because of the deformation of the amorphous parts between spherulites. The cross-section structures of the hollow-fiber membranes fabricated at different drawing ratios are shown in Figure 12. The crystalline particles were stacked, and part of the pore collapsed because of the drawing. Also, the shape of the pores in the cross section changed, and they formed a three-dimensional penetrating structure, which enhanced the connection of holes in the cross section and resulted in an increase in the gas permeability of the hollow-fiber membranes after the drawing.

Th effects of the drawing ratio on the gas permeation are shown in Figure 13. The gas permeation of the hollow-fiber membranes was significantly increased after drawing. The gas permeation of a microporous membrane depends on not only its porosity but also the morphology of its surface. In our case, postdrawing induced a significant open-pore structure on the inner surface, which must have contributed to the gas permeation of the membranes.

Effect of the polymer content

The polymer concentration is an important parameter that affects the membrane structure. It is evident

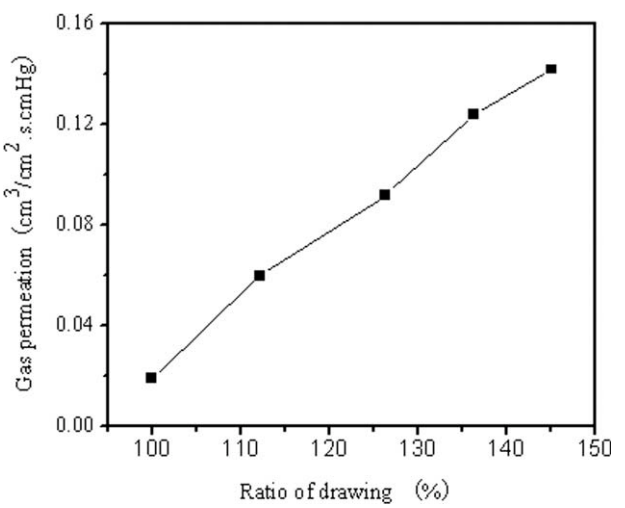

Figure 13 Effect of drawing on the gas permeation of the hollow-fiber membranes.

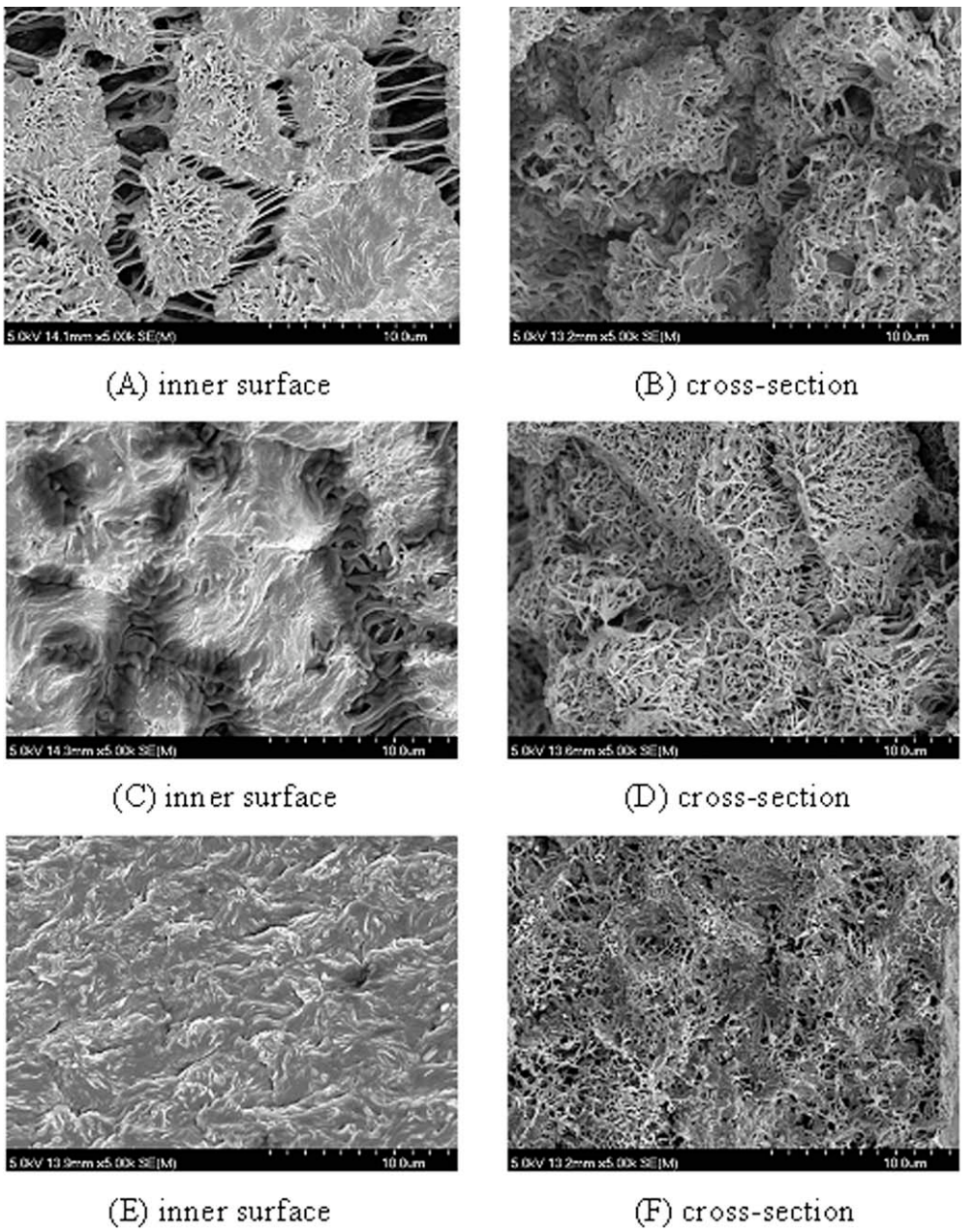

Figure 14 Morphologies of the membranes fabricated with different HDPE contents: (A,B) the 30 wt %HDPE–D/SO system, (C,D) the 40 wt % HDPE–D/SO system, and (E,F) the 50 wt %HDPE–D/SO system (drawing = 145%, air-gap distance = 10 cm, spinneret temperature = 145°C).

that a higher polymer concentration promotes the mutual entanglement of polymer chains and the formation of more compact net structures. Furthermore, the most critical factor is that the phase-separation mechanism of a polymer/diluent system is seriously affected by the initial concentration.

TABLE II
Properties of the Polyethylene Hollow-Fiber Membranes Prepared with the HDPE–D/SO System

Polymer content (wt %)	Outer diameter (μm)	Thickness (μm)	Porosity (%)	Gas permeation (cm^3/cm^2 s cmHg)
30	746	198	43.4	0.124
40	730	188	35.5	0.067
50	712	186	22.9	0.0018

The HDPE–D/SO system was used. The drawing ratio was 145%, the spinneret temperature was 145°C, and the air-gap distance was 10 cm.

Figure 14 shows SEM photographs of the inner surfaces and cross sections of membranes prepared from HDPE–D/SO blends with HDPE contents of 30, 40, and 50 wt %, respectively. All specimens were drawn to 1.45 times. Comparing the images, we can see that from the specimen with a lower HDPE content, a more porous membrane was obtained. Apparently, the coarsening time from liquid–liquid phase separation was longer than that from solid–liquid phase separation. Furthermore, an increase in the polymer concentration brought about a decrease in the distance between particles. An asymmetric membrane with a dense inner surface and a less porous cross section with a more complex net structure was obtained from the 50 wt % sample, as shown in Figure 14(E,F). This was due to a greatly enhanced supramolecular structure generated during solid–liquid phase separation as the polymer concentration was increased.

Other membrane parameters affected by the polymer concentration are listed in Table II. With an increase in the polymer content, the outer diameter of the hollow fibers decreased as the viscosity of the polymer solution increased. From the data in Table II, we can see that the thickness of the membranes was little influenced by the polymer content. Meanwhile, because the liquid–liquid phase separation changed to solid–liquid phase separation, the porosity, average pore size, and gas permeability decreased.

CONCLUSIONS

A Haake machine was applied to determine the rheology behavior of binary diluent/polyethylene blends. The different rheology behaviors of the HDPE–D/SO blends implied liquid–liquid phase separation with subsequent crystallization of the polymer at low initial HDPE concentrations. TVM was used to determine thermodynamic phase diagrams of HDPE–LP and HDPE–D/SO systems. For hollow-fiber membranes fabricated from HDPE–D/SO blends, the inner surface was more porous than the outer surface because of the differences in the cooling rate and the evaporation rate of the diluents. Cold drawing of the hollow-fiber membranes markedly increased their gas permeability. A analysis of the morphologies produced with different drawing rates revealed that an increase in the drawing rate increased the pore size on the membrane surface. With the polymer content increased, a dense surface with lower gas permeability was obtained because the liquid–liquid phase-separation mechanism was changed to solid–liquid phase separation.

References

1. Lloyd, D. R.; Kinzer, K. E.; Tseng, H. S. J Membr Sci 1991, 52, 1.
2. Lloyd, D. R.; Kinzer, K. E.; Tseng, H. S. J Membr Sci 1990, 52, 239.
3. van de Witte, P.; Dijkstra, P. J.; van den Berg, J. W. A. J Membr Sci 1996, 117, 1.
4. Sun, H.; Rhee, K. B.; Kitano, T.; Mah, S. I. J Appl Polym Sci 1999, 73, 2135.
5. Matsuyama, H.; Okafuji, H.; Maki, T.; Teramoto, M.; Kubota, N. J Membr Sci 2003, 223, 119.
6. Wang, J. L.; Ruan, W. X.; Song, Y. L.; Ji, J. B.; Yao, K. J. J Donghua Univ 2006, 23, 59.
7. Matsuyama, H.; Teramoto, M.; Kudari, S.; Kitamura, Y. J Appl Polym Sci 2001, 82, 169.
8. Sun, H.; Rhee, K. B.; Kitano, T.; Mah, S. I. J Appl Polym Sci 2000, 75, 1235.
9. Jeon, M. Y.; Kim, C. K. J Membr Sci 2007, 300, 172.
10. Yoo, S. H.; Kim, C. K. J Appl Polym Sci 2008, 108, 3154.
11. Berghmans, S.; Berghmans, H.; Meijer, H. E. H. J Membr Sci 1996, 116, 171.
12. Matsuyama, H.; Berghmans, S.; Lloyd, D. R. J Membr Sci 1998, 142, 213.
13. Kim, J.; Hwang, J. R.; Kim, U. Y.; Kim, S. S. J Membr Sci 1995, 108, 25.
14. Paul, M. A.; Douglas, R. L. J Membr Sci 2000, 171, 1.
15. Matsuyama, H.; Berghmans, S.; Lloyd, D. R. Polymer 1999, 40, 2289.
16. Matsuyama, H.; Yuasa, M.; Kitamura, Y.; Teramoto, M.; Lloyd, D. R. J Membr Sci 2000, 179, 91.
17. Wang, J. L.; Xu, Z. K.; Xu, Y. Y. J Appl Polym Sci 2006, 100, 2131.